Progress in Propulsion Physics **1** (2009) 205-224
DOI: 10.1051/eucass/200901205
© Owned by the authors, published by EDP Sciences, 2009

INVESTIGATION OF COMBUSTION CHAMBER ACOUSTICS AND ITS INTERACTION WITH LOX/H_2 SPRAY FLAMES

M. Oschwald and B. Knapp

Acoustics of combustion chambers is investigated experimentally in cold flow and hot fire tests. The performance of absorber elements is analyzed in respect to their effect on combustion chamber eigenfrequencies as well as to their damping characteristics. It is shown that predictions of numerical modal analysis of chamber acoustics are in very good agreement with measurements. In hot fire tests, a burning LOX/H_2 spray is acoustically excited with a siren wheel and combustion response is recorded with dynamic pressure sensors and by high-speed visualization of the spray and the flame. Although no combustion instability could be observed, analyzing the temporal and spatial distribution of flame response allowed addressing the question, whether the coupling of acoustics to combustion is via pressure or velocity sensitive processes.

1 INTRODUCTION

The interaction of resonant acoustic excitation of a rocket combustion chamber with combustion processes is challenging designers of rocket engines for a long time. Under specific conditions, the unsteady heat release due to combustion can feed energy into the acoustic excitation and acoustic pressure and velocity fields may reach in a very short time levels that bring the combustion chamber into risk.

Although basic coupling mechanisms leading to instability are known and a lot of experimental and theoretical investigations have addressed the problem in the past [1, 2], a reliable prediction of stability behavior is still not possible. Rocket chamber design with respect to stability still relies by some part on trial and error and experimental stability rating is a must in rocket engine qualification.

The advanced measurement techniques available today and the progress in the capabilities of numerical tools have motivated to address the problem of combustion instabilities again. In a basic experiment designed for the investigation of the interaction of an acoustic wave with LOX/H_2 spray combustion, the

This is an Open Access article distributed under the terms of the Creative Commons Attribution-Noncommercial License 3.0, which permits unrestricted use, distribution, and reproduction in any noncommercial medium, provided the original work is properly cited.

Article available at http://www.eucass-proceedings.eu or http://dx.doi.org/10.1051/eucass/200901205

response of combustion chamber processes to acoustic excitation is investigated. The phenomenology of the response of the spray and the flame is discussed and the question whether the response of the heat release is due to pressure or velocity coupling is addressed.

If a combustion chamber cannot be operated with sufficient stability margins, the application of damping elements may guarantee stable operation. Baffles protruding into the combustion chamber impose specific symmetries incompatible with that of the critical excitation modes. Quarter wave and Helmholtz resonators are used for dissipating acoustic energy [3–6]. Due to the specific experimental setup, the acoustic coupling of quarter-wave cavities with a combustion chamber has also come into focus during the tests. Given below is a short overview on the experimental phenomenology of the resonant modes. Also, the damping of combustors equipped with one absorber or an absorber ring is discussed.

2 EXPERIMENTAL SETUP

2.1 Combustion Chamber

The combustion chamber has been designed to allow experiments with tangential modes having frequencies in a range representative for rocket engines. Cross

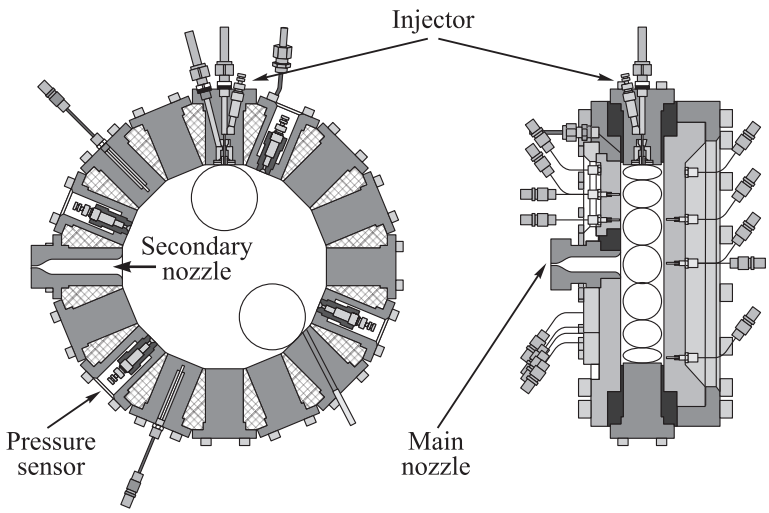

Figure 1 Combustion chamber cross section

sections of the combustor are shown in Fig. 1. The diameter of the chamber is 20 cm, the first tangential mode in hot fire tests is observed at a frequency of about 4 kHz. The length of the chamber is only 4 cm; therefore, the frequency of the first longitudinal mode is expected to be above 17 kHz. Thus, there is no interference of the longitudinal modes with the tangential modes of interest.

Liquid oxygen (LOX) and H_2 are supplied from reservoirs submerged into liquid nitrogen (LN_2). The feed lines and the injector head are cooled by LN_2, thus thermal transients during start-up are minimized and propellant temperatures are near to LN_2-boiling temperature. Liquid oxygen and H_2 are injected in radial direction by a shear coaxial injection element with tapering and without recess.

The combustion gases are released through the main nozzle in axial direction. Nozzles of different diameters can be mounted and with adapting the mass flows tests can be done at chamber pressures between 1.5 and 10 bar.

The flame and the LOX spray are visualized by using a window of 65-millimeter diameter giving optical access to the combustor volume immediately downstream from the injector exit. For specific purposes, a quartz window of 200-millimeter diameter can be mounted giving optical access to the complete combustion chamber volume.

In respect to the radial injection of the propellants and the small length-to-diameter ratio, the concept of the chamber design is similar to that used by Heidmann [7].

2.2 Siren Excitation

Optionally, a secondary nozzle can be mounted as shown in Fig. 2. Through this nozzle, a minor amount of hot gas is released, the mass flow of which can be

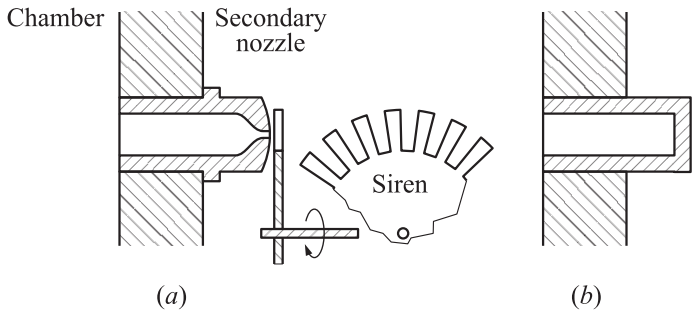

Figure 2 (a) Sketch of the secondary nozzle and the siren wheel; and (b) sketch of a quarter wave cavity

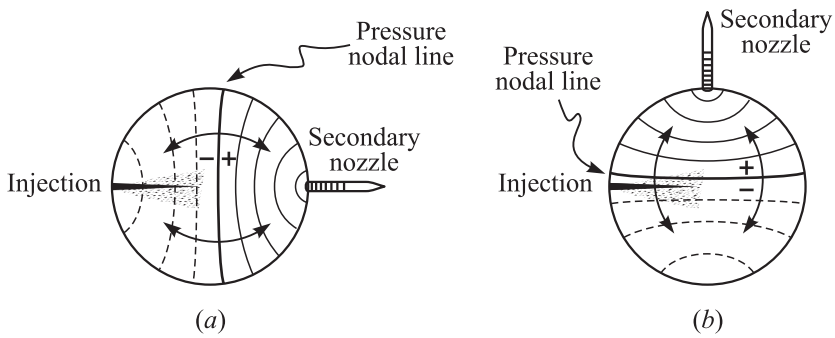

Figure 3 Pressure fields in the combustor for 1T-excitation: (*a*) secondary nozzle at 180° (pressure nodal line perpendicular to the spray axis); and (*b*) secondary nozzle at 90° (pressure nodal line near to and parallel to the LOX spray)

modulated by a siren wheel. The siren wheel is used to excite acoustic oscillations in the combustor at well defined frequencies. Usually, the excitation frequency is scanned over the frequency range of interest during a test with a rate of 400 Hz/s. Excitation levels can reach several percent of the mean chamber pressure at resonance conditions.

The secondary nozzle can be mounted at several angular positions on the circumference of the combustor. As shown in Fig. 3, the angular position controls the orientation of the excited mode relative to the spray axis. Two specific setups have been used. In one configuration, the secondary nozzle has been mounted at the 180 degree position with a pressure antinode at the injector exit (Fig. 3*a*). The acoustic velocity field is parallel to the spray axis in this configuration. In the other configuration, the secondary nozzle has been mounted at the 90 degree position with the LOX-spray near to the pressure nodal line (Fig. 3*b*). The acoustic velocity field is perpendicular to the spray axis and the velocity changes its sign twice a period.

2.3 Sensors and Diagnostics

The pressure in the combustion chamber is recorded during a test by static and dynamic pressure sensors. Up to 6 dynamic sensors are distributed around the circumference of the combustor to resolve the tangential symmetry properties of the excited modes. The data acquisition rate of the dynamic sensors was 27 kHz fulfilling the requirements of the sampling theorem for the modes of interest which have eigenfrequencies between about 4 kHz (1T) and 10 kHz (3T).

The dynamic response of the LOX spray and the flame to acoustic excitation is determined by high-speed visualization techniques. Line-of-sight images

with backlighting of the scene are recorded with a Photron Ultima 1024 C CCD-Camera at 16 000 frames/s and a resolution of 256×32 pixel. For visualization of the flame front, the wavelengths corresponding to the chemiluminescence of the OH-radical near to 307 nm have been selected by an interference filter. An intensified charge-coupled device (ICCD) camera (Photron Ultima I2, 27000 frames/s, resolution 128×64 pixel) is used to detect the spatial distribution of the reaction zone in the combustor. The ICCD camera gives the advantage of spatial resolution but its small dynamic range (8 bit) limits the resolution of small intensity variations. For that reason, a photomultiplier was also used to measure locally the intensity of flame emission.

3 DATA REDUCTION

3.1 Pressure Data

The time series of dynamic pressure data were analyzed by applying a sliding Fast Fourier Transform (FFT). Thus during the run-time of the experiment, the evolution of the eigenmodes of the combustion chamber could be evaluated.

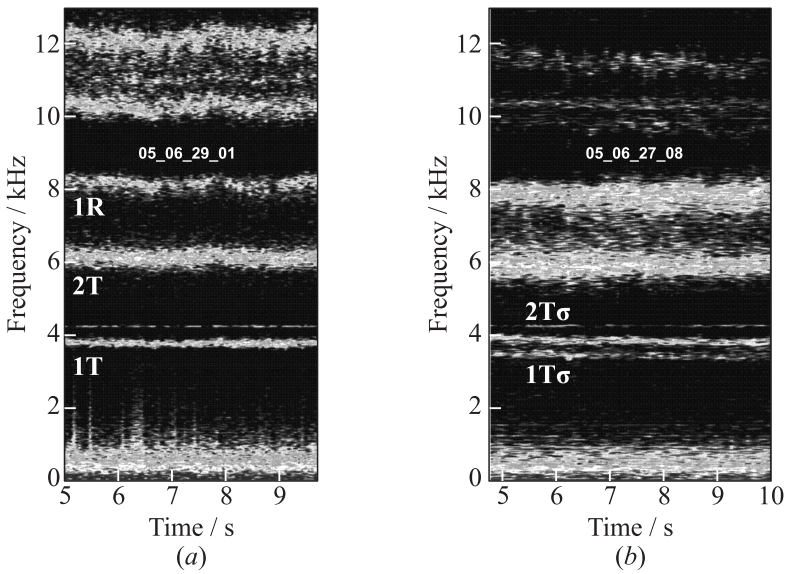

Figure 4 Spectrogram of the combustion chamber pressure noise without (a) and with (b) secondary nozzle

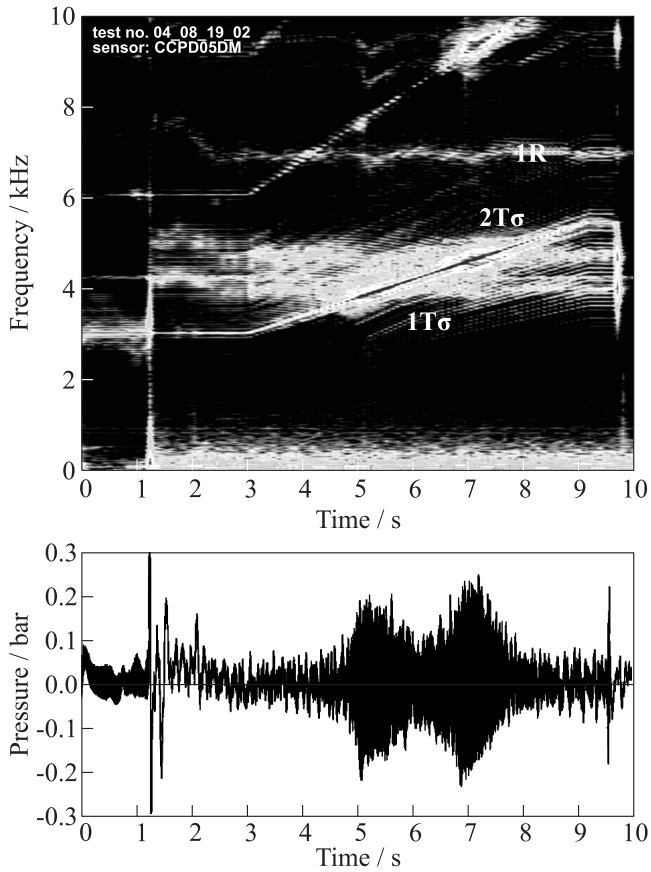

Figure 5 Spectrogram of the combustion chamber pressure during ramping the excitation frequency from 3 to 5.4 kHz

Examples for a test without siren excitation is shown in Fig. 4 for the cases without (a) and with (b) secondary nozzle (SN). With excitation by the siren wheel and ramping of the excitation frequency, the temporally resolved response of the combustion process is given in Fig. 5. The eigenmodes of the combustor can be seen even when the excitation is off-resonance. When the excitation frequency matches one of the eigenfrequencies of the acoustic system, high amplitudes of the dynamic pressures are observed at these frequencies. The peak-to-peak value ΔP of the variation of the dynamic pressure $P'(t)$ on resonance is taken to determine the pressure response $\Delta P/P$. In special cases, a band-pass filter was applied to the pressure data. Finally, the local pressure fluctuations measured by the dynamic sensors were used to reconstruct the amplitude of the acoustic

pressure field $\Delta P(x, y)$ based on the numerically determined pressure distribution of the eigenmode in the resonance volume.

3.2 OH-Imaging

The analysis of the OH-images addressed two aspects: (*i*) the spatial variation of the flame front location, i.e., the movement of the flame in the acoustic velocity field; and (*ii*) the temporal variation of the flame emission intensity, i.e., the heat release response to the acoustic excitation.

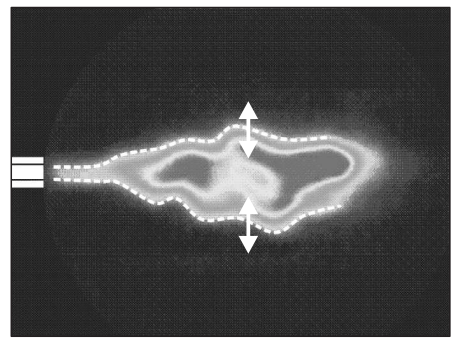

Figure 6 OH-image of the LOX/H_2 spray flame and sketch of flame front as determined with images processing techniques

The acoustic excitation imposes a periodic velocity field on the flow in the combustion chamber and the flame front is convected with this velocity field. The droplets of the LOX spray, however, have only limited ability to follow the acoustic velocity field due to their inertia. A quantitative estimation of the flame front movement does, therefore, not only give information on the level of acoustic excitation but also on acoustically induced relative movement of droplets and surrounding gas. This relative velocity is regarded as a potential driver for combustion/acoustics interaction by velocity-coupled processes like droplet evaporation and secondary atomization. For an excitation with the siren at the 90 degree position as shown in Fig. 3*b*, the acoustic velocity field is perpendicular to the spray axis. Due to the acoustic velocity, the gas and thus, the flame front are convected periodically up and down. The temporal evolution of the flame front position is tracked in the series of OH-images by automated image processing techniques. Thus, the movement of the flame front in the acoustic field in the direction sketched by the arrows in Fig. 6 is evaluated.

A coupling between acoustics and combustion results in a modulation of the heat release $Q(t) = Q + Q'(t)$. The amplitude of the heat release modulation ΔQ and its phase shift relative to the acoustic wave controls whether the coupling leads to an amplification or a damping of the acoustic excitation. This has been firstly discussed by Lord Rayleigh and the condition for amplification is expressed in his famous criterion [8, 9]:

$$\int_V \int_t P'Q' \, dt \, dV > 0 \,. \tag{1}$$

Following Heidmann and Wieber [10], a response factor N can be defined based on the Rayleigh criterion:

$$N = \frac{\int_V \int_t p'q' \, dt \, dV}{\int_V \int_t p'^2 \, dt \, dV} \tag{2}$$

with $q' = Q'/Q$ and $p' = P'/P$. Assuming harmonic time dependencies for $P'(t) = \Delta P \cos(\omega t)$ and $Q'(t) = \Delta Q \cos(\omega t + \phi)$, Eq. (2) reduces to

$$N = \frac{\Delta Q/Q}{\Delta P/P} \cos(\phi) \; . \tag{3}$$

The amplitude ΔQ of the heat release due to the coupling has to be high enough to exceed losses, as, for example, due to the acoustic impedance of the nozzle. Optimum amplification is obtained when the heat release and its associated expansion of the hot gases is in phase with the acoustic pressure ($\phi = 0$), whereas the coupling results in maximum damping of acoustic excitations when $\phi = \pi$. The determination of N requires thus knowledge of the heat release Q and its phase shift ϕ.

In the reaction front of an H_2/O_2 flame, the OH-radical is produced in an excited electronic state and the intensity $I(t) = I + I'(t)$ of the chemiluminescence of this radical is taken as a qualitative measure for the heat release $Q(t)$. The amplitude ΔI of the OH-intensity variation is identified with the heat release fluctuation ΔQ due to the coupling of the acoustics with the combustion process. The heat release fluctuation in Eq. (3) is substituted with the fluctuation of the flame emission intensity $\Delta I/I$. By the simultaneous measurement of the dynamic pressure and the OH flame emission, a response factor can thus be determined:

$$N = \frac{\Delta I/I}{\Delta P/P} \cos(\phi) \, . \tag{4}$$

Each image of the image sequence recorded with the high-speed ICCD camera is analyzed locally in specific regions of interest. In each of these regions, the spatial mean gray value $I(x, y)$ is evaluated. From the image sequence, thus, the spatially resolved evolution of the OH-intensity $I(t; x, y) = I(x, y) + \Delta I(x, y) \cos(\omega t + \phi)$ can be determined. The amplitude of the flame response $\Delta I(x, y)$ at frequency ω is determined with a similar procedure as in the case of the dynamic pressure. From these local intensity data and the pressure field reconstructed from the dynamic-pressure sensor measurements, a local response factor can be evaluated.

3.3 Spray Visualization

A simple approach has been used to analyze the sequence of spray images for a potential dynamic spray response on the acoustic field. As shown in Fig. 7, two regions of interest have been defined. The mean gray value in either of these regions is evaluated for each image and for each region time series of gray values are obtained. For an excitation as shown in Fig. 3*a*, the acoustic velocity is directed parallel to the jet axis and a dynamic response of the liquid due to the drag of the acoustic velocity field should result in a periodic modulation of the liquid flow in this direction. In the FFT of the time series of gray values for the region of interest shown in the upper spray image in Fig. 7, a peak at the acoustic frequency is expected. The response for the region of interest in the lower image of Fig. 7 should be less sigificant in this case. For an excitation as shown in Fig. 3*b*, the acoustic velocity is directed perpendicular to the jet axis. In this case, the time series for the region of interest in the lower image of Fig. 7 should be sensitive to the excitation frequency whereas the region of interest in the upper image should not.

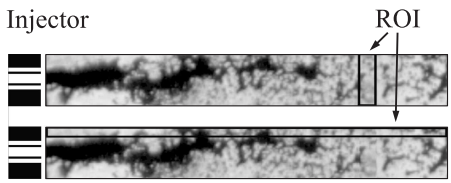

Figure 7 Visualization of the LOX spray and regions of interest for the analysis of periodic variations in horizontal (top) and vertical (bottom) direction

4 EXPERIMENTAL RESULTS

4.1 Acoustic Resonances of Combustor with External Excitation

Resonance frequencies

The inlet of the secondary nozzle forms a cavity adding a complementary volume to the combustor with similar acoustic properties as an absorber cavity (see Fig. 2). The eigenfrequencies of the coupled acoustic system formed by the secondary nozzle inlet cavity and the combustor deviate significantly from that of the combustor alone, an observation which has first been done and explained by G. Searby at the CNRS in Marseille. The analogy of the inlet cavity and a quarter wave cavity motivated a more detailed analysis of the phenomenon.

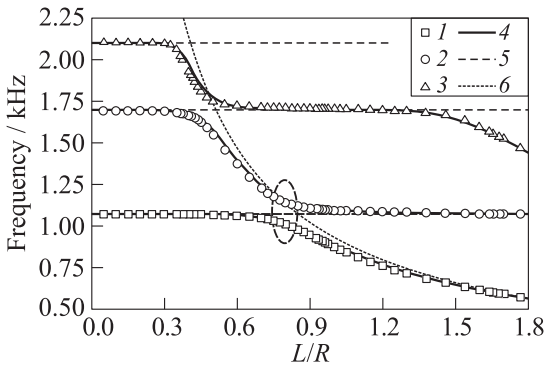

Figure 8 Eigenfrequency of a combustor with absorber cavity as a function af cavity length: *1* — 1Tσ (experiment); *2* — 2Tσ (experiment); *3* — 1R (experiment); *4* — σ-modes (numerical); *5* — π-modes (numerical); and *6* — $\lambda/4$ resonance

Only the general phenomenology is presented here, a detailed analysis has been given elsewhere [11].

In Fig. 4, spectrograms of the combustion noise in the combustor without and with SN are shown. Whereas in the case without SN resonances at frequencies of the well-known cylinder modes 1T, 2T, 1R, etc. are seen, the application of the secondary nozzle changes the resonance behavior, especially near the frequency of the 1T-mode. New frequencies appear which are labeled 1Tσ and 2Tσ in Fig. 4. The ratio of the length of the secondary nozzle L to the radius R of the combustor was about $L/R \approx 0.8$ in the experiments.

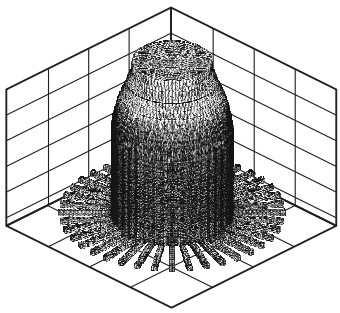

Figure 9 Mesh used for a modal analysis of a rocket combustor with absorber ring

More insight in the situation has been obtained by a numerical modal analysis of the coupled acoustic system. The result of such an analysis with the combustor filled with ambient air is shown in Fig. 8. When a cavity is coupled to a cylindrical combustor, the cylindrical symmetry is broken and as a consequence, the tangential eigenmodes are no more twofold degenerate. With increasing cavity length L, the resonance frequency of one of the two components of a tangential mode is rather not influenced by the cavity, whereas the other is detuned to lower frequencies. These two components are labeled π and σ, respectively. In Fig. 8, it is obvious that for $L/R \approx 0.8$, the detuned σ-components of the 1T- and 2T-modes form the line doublet near the

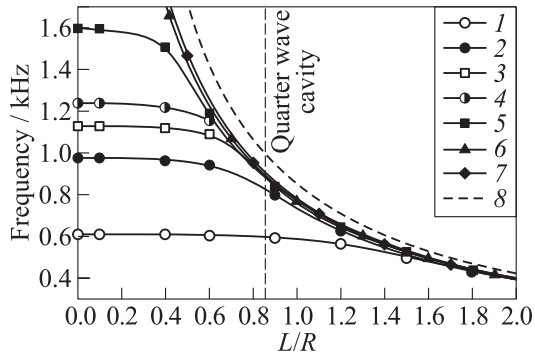

Figure 10 Eigenfrequencies as function of the absorber length L for a combustor with a cavity ring of 42 absorbers: *1* — 1L; *2* — 1T; *3* — 2L; *4* — 1T1L; *5* — 2T; *6* — 3T; *7* — 4T; and *8* — $f = c/(4L)$

1T-frequency as seen on the spectrogram on the right-hand side of Fig. 4. The sensor was positioned on the nodal line of the $1T\pi$-mode and was, therefore, not observed in the measurement.

The observation of detuning of the cylindrical eigenmodes when applying an individual absorber rises the question on the effect of an absorber ring. The first few eigenmodes with lowest frequencies have been analyzed for a combustor with 42 absorbers with a numerical three-dimensional (3D) modal analysis (Fig. 9). As shown in Fig. 10, all the eigenmodes investigated are detuned by the absorber ring and their eigenfrequencies are below that of the quarter wave resonance of the absorbers.

Line profiles

The Fourier transform of a harmonic oscillation of fixed frequency and infinite duration would result in a δ-function. In a combustor, acoustic waves are damped due to acoustic dissipation and the free evolution of the acoustic waves is distorted due to the interaction with the combustion processes. Damping and interactions result in a finite line width of the Fourier-transformed signal and the shape and width of the resonance profile contains information on the interaction of the wave with its environment. For a damped harmonic oscillator, the Fourier transform delivers a Lorentzian line profile with its full width at half maximum corresponding to the damping coefficient.

The observation that the coupling of a cavity with the combustor is detuning the acoustic system has motivated not only to investigate experimentally the resonance frequencies but as well the damping behavior of quarter-wave cavity. These tests have been done under cold flow conditions to provide well-defined

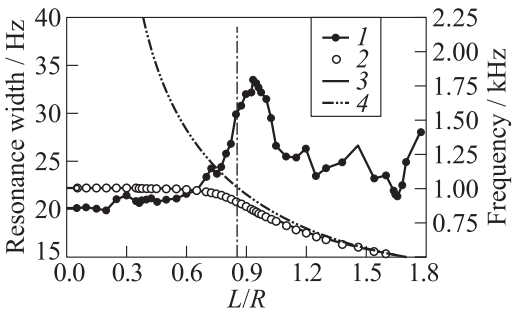

Figure 11 Line width (*1*) and resonance frequency for the 1Tσ-resonance as functions of the resonator length: *2* — 1Tσ (experiment); *3* — CFD; and *4* — $\lambda/4$ resonance

experimental conditions and are described in detail elsewhere [11]. Only one example of data for a cavity of 12.3-millimeter diameter coupled to the combustor is given here.

In Fig. 11, the line width, i.e., damping of the 1Tσ-mode is shown as function of the cavity length. The dash dotted vertical line is marking the length $L/R = 0.85$, where the quarter-wave resonance $f_{\mathrm{QW}} = c/(4L)$ of the absorber would correspond to the 1T-frequency of the combustor without absorber. As clearly seen, the highest damping is not observed for an absorber of this length but at a larger value of L.

In Fig. 12, the resonance profiles for the 1Tσ- and 2Tσ-modes are shown under cold flow conditions but with an otherwise identical configuration as in the hot-fire tests. The combustion chamber was purged with N_2 and the chamber was excited using the exciter wheel.

As can be seen in Fig. 12, the envelope of the resonance profile is in good agreement with a Lorentzian. The full width at half maximum is ≈ 16 Hz. The "noisy" appearance of the profile when exciting with the siren is reproducible and is not seen when the combustor is excited under cold flow conditions with a loudspeaker [11]. The reason for this deviation from a Lorentzian resonance profile is not finally clarified but it seems to be related to the siren excitation mechanism. There is indication that together with the 1Tσ-mode, simultaneously, a spinning mode may be excited.

Resonance profiles for hot fire conditions are shown in Fig. 13. The profiles are strongly disturbed, the 1Tσ-peak is asymmetric and its envelope does not show a Lorentzian shape. Deviations from Lorentzian line shapes are much more pronounced as compared to the cold-flow tests. The line width of the 1Tσ mode is 233 Hz, significantly wider than under cold flow conditions and thus giving clear indication for an interaction of the acoustic wave with the combustion process.

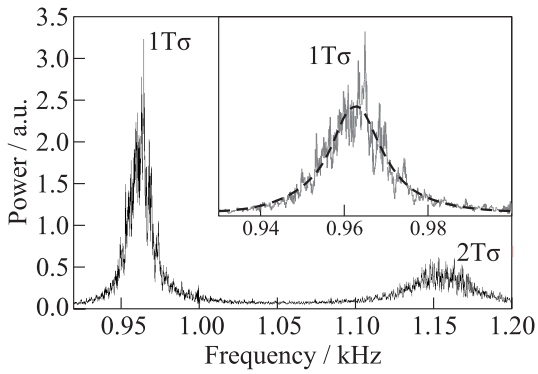

Figure 12 Line profiles for cold flow conditions. Dashed curve corresponds to Lorentz fit

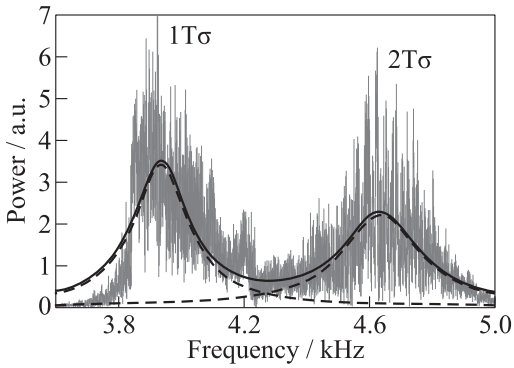

Figure 13 Line profiles for hot fire conditions. Curves correspond to Lorentz fit

4.2 Coupling of Acoustics with Spray Combustion

Dynamics of the LOX/H_2 spray flame

OH-Emission The spontaneous emission of the flame in the wavelength range of OH-radical chemiluminescence is used to analyze coupling of the flame with the acoustics in several aspects: The spatial distribution of the flame emission is used to track the position of the flame front of the LOX/H_2 spray flame and the emission intensity is taken as a qualitative measure for the heat release.

According to the Rayleigh criterion, a key parameter controlling whether coupling between acoustics and heat release results in amplification or damping of the acoustic wave, is the phase shift ϕ between pressure and heat release

fluctuations. As seen from Eq. (4), maximum amplification is obtained when heat release and pressure fluctuations are in phase, i.e., $\phi = 0$. In experiments reported herein, the phase shift has been proved to be zero in the frame of the measurement accuracy indicating a positive coupling of acoustics with combustion.

The high data acquisition rate of the camera used for flame emission imaging allowed resolving the movement of the flame in the acoustic velocity field. Here, the case with siren excitation at the 90 degree position (see Fig. 3*b*) is discussed. In this configuration, the acoustic velocity vector is perpendicular to the spray axis, and the gas is convected periodically in the upward and downward direction. For discussing the main features, the interaction of the acoustic wave with the combustion process is neglected and it is assumed that the flame front is convected with the acoustic velocity. However, LOX-droplets, because of their inertia, hardly follow the acoustic velocity fluctuations. The characterization of flame front movements gives therefore access to the relative velocity between gas phase and liquid droplets imposed by the acoustics. This data can be used to address the interaction processes between acoustics and combustion due to velocity sensitive processes like secondary atomization and droplet evaporation.

In a burning LOX/H_2 spray flame, the flame front forms a cone around the core of the atomized LOX-spray and evaporating LOX-droplets. Due to the progress of LOX evaporation downstream from the injector exit and the production of hot reaction products, the diameter of this flame-cone is expanding immediately downstream from the injector exit as can be seen in Fig. 6. In the transversal acoustic velocity field, this flame cone is moving synchronously up and down. For several positions downstream from the injector exit, the movement of the flame front in the upward and downward direction has been tracked and the flame front position has been evaluated as a function of time. From these

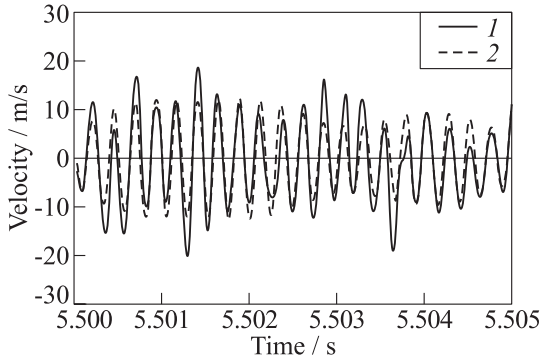

Figure 14 Transversal flame front movements during acoustic resonance: *1* — raw data and *2* — FFT filtered 3.5–4.5 kHz

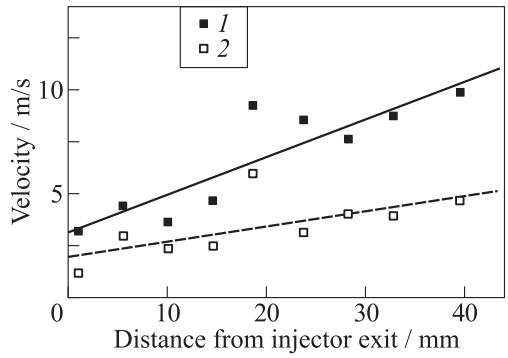

Figure 15 Root mean square values of the transversal flame front movement: *1* — raw data and *2* — FFT filtered 3.5–4.5 kHz

data, the velocity of the flame front movement in the acoustic field has been determined.

The result is plotted in Fig. 14 for a distance from the injector of $x = 18.6$ mm. The movement due to the acoustic field is clearly resolved by this method and a typical amplitude of ≈ 9 m/s is observed. The flame front oscillates, however, not with constant amplitude and maximum values of up to more than 25 m/s can be observed at this location. During the time of data acquisition, the dynamic pressure sensors show a constant amplitude of pressure oscillations; thus, this should be true as well for the acoustic velocity field. The variation in the amplitude of the flame front movement is attributed to the dynamics of the mixing layer, the combustion process, and local turbulence. The flame front movement due to these effects is superimposed on the movement due to the acoustic field. To reduce the contribution of these effects, the raw-data have been band-pass filtered around the excitation frequency. The filtered data in Fig. 14 show a reduced variance of the amplitudes. To quantify the flame front movement, the root mean square (rms) values of the flame-front velocity fluctuations during 5 ms, i.e., about 20 acoustic periods, have been evaluated at several distances from the injector. As shown in Fig. 15, the amplitudes are increasing with increasing distance from the injector exit. The larger slope of the raw-data as compared to the filtered data can be understood in view of the increasing size of vortices in the mixing layer and their influence on the flame front contour with increasing distance from the injector. The flame front movement evaluated from the filtered data is much smaller than the estimated acoustic velocity based on the dynamic pressure measurement.

Spray Visualization. For two regions of interest in the backlighting images, the time series of mean gray values have been evaluated as described in sec-

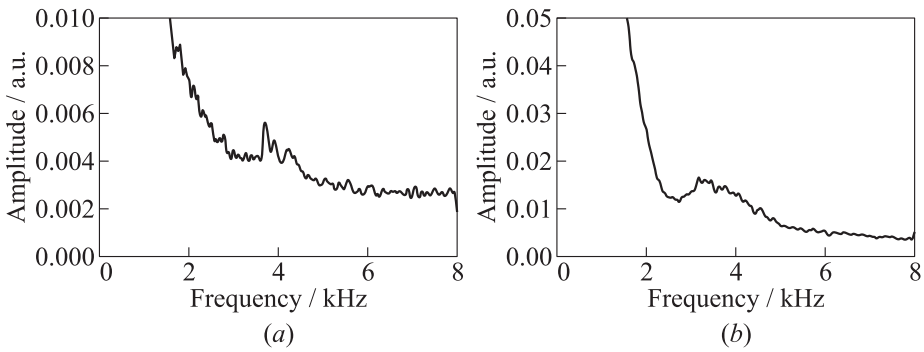

Figure 16 Fourier-transform of the mean gray values of the region of interest sensitive to vertical (a) and horizontal (b) oscillations

tion 3.3. For an excitation with the siren wheel at 90°, a small response at the frequency of the acoustic excitation is observed in the vertical (Fig. 16a) as well as in the horizontal direction (Fig. 16b). The response in vertical direction could be expected due to the vertically directed acoustic velocity for this test-setup. The response observed in the area of interest sensitive to horizontal oscillations, however, is even stronger.

Two-dimensional distribution of combustion response

The acoustic pressure and velocity fields have characteristic spatial distributions (see Fig. 3) and the analysis of the flame emission response as a function of the orientation of the pressure nodal line is used to address the question whether the flame is coupled to the acoustic velocity or to the acoustic pressure.

Without secondary nozzle (and, thus, no external excitation), a low-level acoustic field is observed with 1T-symmetry and a pressure nodal line perpendicular to the injection axis (similar to Fig. 3a). Thus, the mode with its maximum pressure oscillation in the spray region near the injector, the region of primary atomization, evaporation of liquid, and flame stabilization is preferred. This is the first indication that energy from combustion is transferred into the acoustic 1T-mode by pressure coupling.

The temporal evolution of the flame emission has been recorded by the ICCD-camera. From these data, the mean emission intensity I and the amplitude of the intensity fluctuation ΔI are determined. The value of the relative oscillation of the chemiluminescence response $\Delta I/I$ with external excitation has been compared for the siren mounted at the 180 degree position (Fig. 3a) and the 90 degree position (Fig. 3b). Based on mean values from several tests, it is concluded that with external excitation, a higher relative oscillation of the chemiluminescence

response $\Delta I/I$ is observed in the spray with the siren at the 180 degree position as compared to the excitation at 90°. Thus, a higher dynamic response of the flame emission is induced when the pressure antinode is in the spray region (as sketched in Fig. 3*a*). This is another indication for a pressure coupling of combustion and acoustics.

To compare the spatial distribution of the flame response $\Delta I(x, y)/I(x, y)$ with the spatial symmetry characteristics of the excited mode $\Delta P(x, y)/P(x, y)$, the large window has been mounted to get optical access to the complete combustor volume. Due to the limitation of the spatial resolution of the high-speed ICCD-camera only the flame in the lower part of the combustor is visualized. For the image series, the local temporal evolution of flame intensity is evaluated; thus, the local mean $I(x, y)$ and its fluctuation amplitude $\Delta I(x, y)$ at the excitation frequency could be determined. Correspondingly, from the dynamic pressure recordings the amplitude distribution $\Delta P(x, y)/P(x, y)$ of the excited eigenmode is reconstructed. From these data with the help of Eq. (4), a local response factor has been evaluated for the configuration with the siren at the 90 degree position. The data have been recorded when the chamber was excited at the 1Tσ-mode.

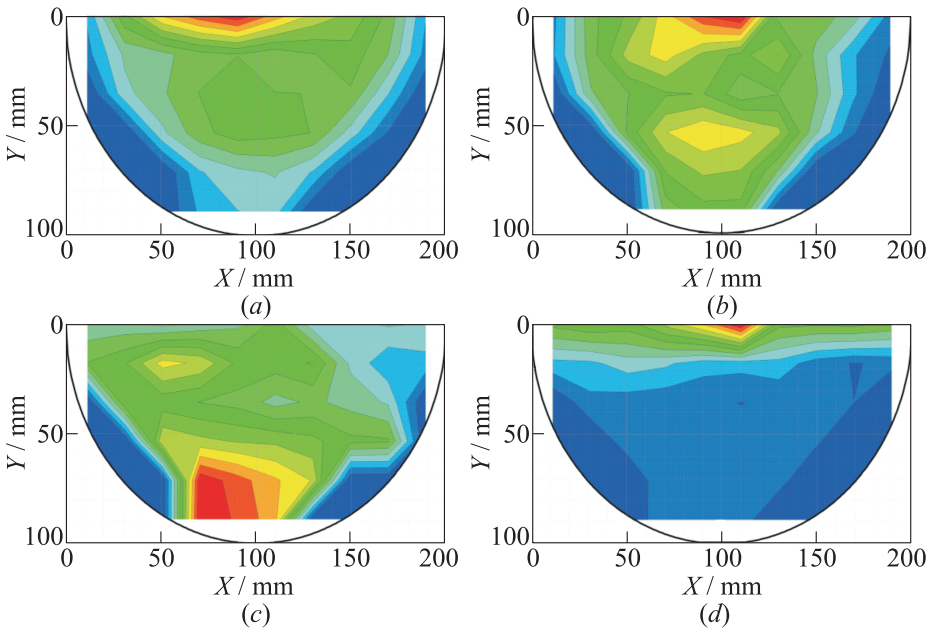

Figure 17 Local mean flame intensity and flame response for excitation with siren at 90°: (*a*) mean intensity I; (*b*) intensity fluctuation ΔI; (*c*) relative flame response $\Delta I/I$; and (*d*) response factor N. (Refer Oschwald and Knapp, p. 221.)

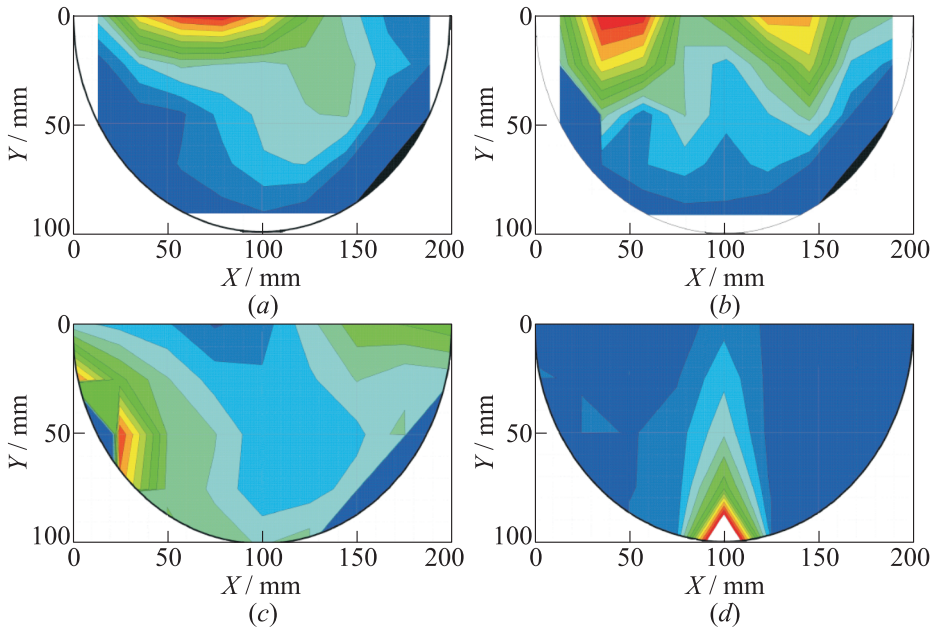

Figure 18 Local mean flame intensity and flame response for excitation with siren at 180°: (*a*) mean intensity I; (*b*) intensity fluctuation ΔI; (*c*) relative flame response $\Delta I/I$; and (*d*) response factor N. (Refer Oschwald and Knapp, p. 222.)

In Fig. 17*a*, the mean value I and in Fig. 17*b* the amplitude ΔI of the flame emission are shown for excitation with the siren at 90°. Both distributions show high values on the spray axis. Maximum variation of the flame emission ΔI is seen where the flame has maximum intensity. The relative flame response $\Delta I/I$ (Fig. 17*c*) exhibits no maximum on the spray axis: near the pressure nodal line, the relative I-variation is small and the maximum is observed where there is the pressure antinode. Thus, the spatial distribution of $\Delta I/I$ reflects the pressure distribution of the excited 1T-mode for siren excitation at 90° (see Fig. 3*b*).

For excitation with the siren at the 180 degree position (see Fig. 3*a*), the results are shown in Fig. 18. The mean flame intensity is very similar as in the case of 90 degree excitation, maximum intensity is seen on the spray axis (Fig. 18*a*). The variation of the flame emission ΔI (Fig. 18*b*) and the relative flame response $\Delta I/I$ (Fig. 18*c*) again reflects the symmetry of the acoustic pressure field, now for 180 degree excitation: minimum values are observed on the presure nodal lines, maximum values — in the regions of the pressure antinodes. From these observations, it is concluded that for the conditions of the experiment, there is

coupling of the LOX/H_2 spray flame with an acoustic wave and the coupling process is pressure sensitive.

The local response factor $N(x, y)$ is shown in Figs. 17*d* and 18*d*. For the excitation at 90°, a maximum is found on the spray axis, which is in agreement with expectations because sensitive processes (droplet vaporization, chemical reaction) are located in that region. However, for the 180 degree excitation, the result for the response factor does not show a similar reasonable distribution. The accuracy of the response factor determination is limited due to low data quality. The value of $N = (\Delta I/I)/(\Delta P/P)$ near the pressure nodal line is very sensitive to the assumed location of the nodal line where $\Delta P \sim 0$. The accuracy of the measurements has to be improved for a quantitative evaluation of N.

5 SUMMARY AND CONCLUDING REMARKS

In cold and hot fire tests, it has been observed that the coupling of a cavity with a cylindrical combustor results in detuning of the acoustic system. The eigenmodes of the combustor with a cavity or a cavity ring do not correspond any more to the well-known eigenmodes of cylindrical resonators.

By applying high-speed visualization techniques, the coupling of acoustic waves with the LOX spray and with the LOX/H_2 spray flame has been investigated. According to the Rayleigh criterion, the zero phase shift measured between the dynamic part of the flame emission and the acoustic pressure confirms a positive coupling in the experiments leading to instability if combustion gain is higher than the losses. However, in present experiments, no sustainable acoustic oscillation has been observed without external excitation with the siren wheel.

Based on the comparison of the symmetry of the observed flame response and the symmetry of the excited acoustic mode, it is concluded that the acoustic field and the combustion process are coupled by a pressure sensitive process rather than by a velocity sensitive process.

REFERENCES

1. Harrje, D. T., and F. H. Reardon. 1972. Liquid propellant rocket combustion instability. NASA SP-194.
2. Yang, V., and W. E. Anderson, eds. 1995. *Liquid rocket engine combustion instability*. Progress in astronautics and aeronautics ser. AIAA Inc. 169.
3. Oberg, C. L., T. L. Wong, and W. M. Ford. 1971. Evaluation of acoustic cavities for combustion stabilization. NASA CR 115087.

4. Laudien, E., R. Pongratz, R. Pierro, and D. Preclik. 1995. Experimental procedures aiding the design of acoustic cavities. In: *Liquid rocket engine combustion instability*. Eds. V. Yang and W. Anderson. Progress in astronautics and aeronautics ser. AIAA Inc. 169:377–99.
5. Frendi, A., T. Nesman, and F. Canabal. 2005. Control of combustion-instabilities through various passive devices. AIAA Paper No. 2005-2832.
6. Richards, G. A., D. L. Straub, and E. H. Robey. 2005. Passive control of combustion instabilities in stationary gas turbines. In: *Combustion instabilities in gas turbine engines*. Eds. T. C. Liuwen and V. Yang. Progress in astronautics and aeronautics ser. AIAA Inc. 210.
7. Heidmann, M. F. 1965. Oscillatory combustion of a liquid-oxygen jet with gaseous hydrogen. NASA TN-D-2753.
8. Lord Rayleigh. 1878. The explanation of certain acoustical phenomena. *R. Inst. Proc.* VIII:536–42.
9. Lord Rayleigh. 1945. *The theory of sound*. New York: Dover. II:226.
10. Heidmann, M. F., and P. Wieber. 1966. Analysis of frequency response characteristics of propellant vaporization. NASA TN-D-3749.
11. Oschwald, M., Z. Farago, G. Searby, and F. Cheuret. 2008. Resonance frequencies and damping of a combustor acoustically coupled to an absorber. *J. Propul. Power* 24(3):524–33.